J Appl Electrochem (2010) 40:419–425
DOI 10.1007/s10800-009-0012-2

ORIGINAL PAPER

A novel synthesis of Fe_2P–$LiFePO_4$ composites for Li-ion batteries

Youyong Liu · Chuanbao Cao · Jing Li · Xingyan Xu

Received: 16 February 2009 / Accepted: 2 September 2009 / Published online: 15 September 2009

Abstract Fe_2P–$LiFePO_4$ composites were synthesized by a novel method consisting of co-precipitation modified with in situ polyacrylamide (PAM) formation. Simultaneous thermogravimetric-differential scanning calorimetric analysis indicated that the in situ PAM precursor exhibited a moderate continuous weight loss rather than a sharp mass loss process. The best Fe_2P–$LiFePO_4$ composite was obtained from 14 wt% in situ PAM precursor under a sintering temperature of 750 °C for 20 h, which delivered a discharge capacity of 131 mAh g^{-1} at a rate of C/5 and 110 mAh g^{-1} at 1 C and sustained 30 cycles with almost no capacity fading. The relatively good electrochemical performance originates mainly from the well-mixed gelation precursor and conductive Fe_2P phase with better electronic conductivity. This novel method verified that the electrochemical performance was improved compared to the conventional $LiFePO_4$ without in situ PAM. It can be anticipated that the same process should be readily extendable to other olivines, such as $LiMnPO_4$ and $LiCoPO_4$, and also to other phosphates.

Keywords Li-ion batteries · $LiFePO_4$ · Fe_2P · Co-precipitation · Polyacrylamide

1 Introduction

Portable power applications continue to drive research and development of advanced energy storage devices, especially the sustainable, environmentally benign ones [1]. In recent years, considerable attention has been focused on electronic vehicles and hybrid electronic vehicles in an attempt to relieve the pressure from global warming. Among the available devices, lithium-based batteries are the most promising candidate in terms of high energy density and lower toxicity. Cobalt-based materials have been prevented from widespread use because of environmental harm and lack of safety. Fe- and Mn-based materials are very attractive due to their low cost and low toxicity. However, Mn-based materials suffer from poor cycling stability, especially at high temperature [2].

One of the most promising Fe-based materials is $LiFePO_4$, and intensive studies have focused on $LiFePO_4$ materials with olivine structure since the pioneering work presented by Padhi et al. [3]. $LiFePO_4$ has a large theoretical capacity of 170 mAh g^{-1}, excellent cycling stability, and acceptable operating voltage (3.45 V vs. Li^+/Li). Moreover, $LiFePO_4$ is abundantly available and environment friendly. Although it possesses such advantages, $LiFePO_4$ still meets some obstacles for commercial utilization. One of the main drawbacks of $LiFePO_4$ is low electronic conductivity and slow lithium ion diffusion, which results in initial capacity loss and poor rate capacity. In order to overcome these problems, there are two main strategies. One strategy is to introduce conductive additives including carbon nano-coatings [4, 5], metal powder addition [6, 7], metal doping [8], and metal-rich phosphides [9–12]. In view of the above attempts, the incorporation of conductive metal-rich phosphides (Fe_2P) into active material powders to form Fe_2P-coated $LiFePO_4$ (Fe_2P–$LiFePO_4$) seems to be a promising method to overcome the poor rate capacity, because the homogeneous Fe_2P coating on the surface of $LiFePO_4$ particles provides a pathway for electron transfer, enhancing the electronic conductivity. Another strategy for improving the rate performance of

Y. Liu · C. Cao (✉) · J. Li · X. Xu
Research Center of Materials Science, Beijing Institute of Technology, Beijing 100081, People's Republic of China
e-mail: cbcao@bit.edu.cn

$LiFePO_4$ materials is to enhance the ionic/electronic conductivity by minimizing particle size with suitable preparation procedures. Besides the traditional solid-state reaction synthesis routine [13], alternative synthesis processes, including sol–gel [14], hydrothermal [15], emulsion-drying method [16], co-precipitation [7, 17], etc., have been developed. Of these solution methods, the co-precipitation method for synthesizing $LiFePO_4$ has some advantages, such as simple synthesis process and low energy consumption, which can also afford intimate mixing of starting ingredients at the atomic level, thereby allowing fine particles of high purity to be produced by rapid homogeneous nucleation.

Recently, polymer gels have become highly promising as templates for the in situ synthesis of smaller size nanoparticles, and this strategy has created a new concept in hybrid or composite systems in chemistry and engineering science [18–20]. Having taken this advantage, Yang et al. [21] used polyacrylamide (PAM) as a soft template for synthesis of conductive-nanostructured $LiFePO_4$/C. They reported that $LiFePO_4$/C from a pyrolyzed PAM exhibited a capacity of about 113 mAh g^{-1} at C/6. However, simply mixing PAM and raw material could not provide the homogeneous precursor; therefore, the rate capability of the obtained material was not as high as expected. In contrast, in situ PAM formation seems to be a better approach to obtain the well-mixed precursor due to the PAM gelation reaction. In this article, we describe a novel method followed by sintering to prepare Fe_2P–$LiFePO_4$ composites. This synthesis method involved coating the pre-made co-precipitation with in situ PAM through a gelation reaction that made the obtained precursor more uniform. Moreover, the in situ PAM can facilitate the presence of a highly reducing atmosphere during the sintering process, which was crucial for a successful preparation of Fe_2P phase on the surface of $LiFePO_4$. We optimized the synthesis conditions and examined the relationship between the synthesis conditions and the electrochemical properties. For comparison, $LiFePO_4$ without the in situ PAM (denoted as the conventional PAM sample) was also synthesized.

2 Experimental

Fe_2P–$LiFePO_4$ composites were prepared by the following steps. First, the co-precipitation mixture was obtained by adding $LiOH{\cdot}H_2O$ solution to the starting mixed materials of LiH_2PO_4 and $FeSO_4{\cdot}7H_2O$. The obtained fresh co-precipitation and acrylamide monomer were mixed in 15 mL of water under vigorous stirring at room temperature. Then, the cross linker *N*,*N*′-methylene bis acrylamide was added into the solution (denoted as M1), with the cross linker and acrylamide at a ratio of 1:5. Azobisizobutyronitril (AIBN) as an initiator was added into a mixed solution of ethanol and acetone with a ratio of 1:1, which was stirred until the AIBN was completely dissolved (denoted as M2). The two solutions (M1 and M2) were mixed under stirring at 70 °C until a highly viscous solution was formed. The wet gel-like mixture was placed in an oven and heated at 70 °C for 12 h. The as-prepared gel-like mixture was ground and then sintered at selected temperatures in an argon atmosphere. For comparison, the conventional PAM sample was also prepared by sintering a simple mixture of the commercial PAM and raw material under the same conditions.

The combined thermal analysis (TG–DSC) of the gel-like mixture was performed in pure N_2 on a Q600 Simultaneous DSC–TGA at a heating rate of 10 °C min^{-1}. The X-ray diffraction (XRD) patterns of $LiFePO_4$ samples were obtained using a PANalytical X-pert diffractometer (PANalytical, Netherlands) with CuK_α radiation operated at 40 kV and 30 mA. Hitachi field-emission scanning electron microscopy (FE-SEM S-4800) measurements were used to observe the particle size and morphology. The residual carbon content of the powders was determined by means of an elemental analyzer (Elementar Vario Micro Cube). The electrochemical properties of the samples were assessed using CR2025 coin cells. The electrodes were prepared by casting and pressing a mixture of 75 wt% of the as-synthesized material, 20 wt% of carbon black, and 5 wt% of poly(vinylidene fluoride) (PVDF) binder in *N*-methyl-2-pyrrolidon (NMP) on aluminum foil followed by drying in vacuum at 120 °C for 12 h. The typical active material loading was 2–3 mg cm^{-2}. The cells were assembled in an argon-filled glove box with lithium metal as the anode and Celgard 2325 film as a separator. The electrolyte was the solution of 1 M $LiPF_6$ dissolved in ethyl carbonate/dimethyl carbonate (EC/DMC) (1:1 volume ratio). Charge–discharge testing was performed galvanostatically at different C rates between 2.5 and 4.2 V on a LAND CT-2000A cell test instrument at room temperature.

3 Results and discussion

3.1 Physical characterization

Thermal gravimetry and differential scanning calorimetry (TG–DSC) was used to determine the temperature for preparation of the precursor. Herein, the combined thermal analysis (TG–DSC; Fig. 1) on the gel-like precursor was examined in the temperature range from room temperature to 800 °C in pure N_2 atmosphere. The DSC curve showed a small exothermic peak at 465 °C, which was related to the transformation from an amorphous to a crystalline phase of the $LiFePO_4$ compound. In the TG curve, the weight loss of

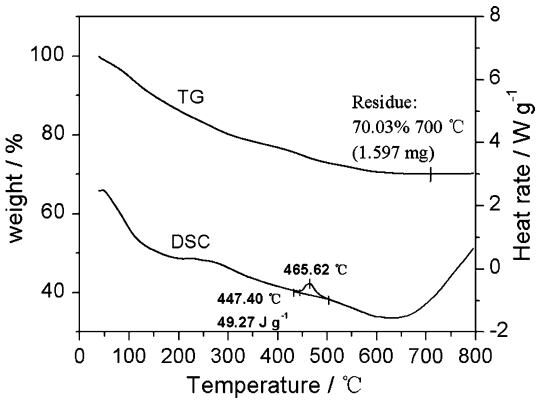

Fig. 1 TG–DSC curves of Fe_2P–$LiFePO_4$ precursor at a 10 K min^{-1} heating rate in N_2 atmosphere

15% before 200 °C corresponds to the release of the physically adsorbed water. As the temperature increases from 200 °C up to 600 °C, the TG curve displayed a weight loss of 14%, which may correspond to the decomposition of PAM gel in the gel-like precursor. It was noteworthy that the gel-like precursor did not show a sharp weight-loss process as reported previously in the literature [22], but exhibited a moderate continuous weight loss. This implied that the gel-like precursor decomposed gradually rather than evaporated rapidly during the successive thermal treatment. Above 600 °C, the weight remained almost constant, indicating that the phase transformation was completed. On the basis of the results of TG–DSC analysis, the synthesis temperature of the well-crystallized $LiFePO_4$ should be chosen to be above 600 °C.

In order to synthesize Fe_2P–$LiFePO_4$ composites successfully, the generation temperature of Fe_2P in the bulk must be determined. The gel-like precursor with 14 wt% PAM was sintered at the temperatures from 650 to 750 °C, and XRD patterns of the obtained samples are shown in Fig. 2a. Obviously, the samples sintered at 650 and 700 °C showed an olivine-type structure with the Pnma space group without detectable impurities. For the sample prepared at 750 °C, an olivine-type structure was maintained upon increasing the temperature, but a minor impurity phase, which was indexed to be iron phosphide (Fe_2P), was observed. The presence of the impurity Fe_2P peak in the XRD pattern (Fig. 2a) showed that the Fe_2P phase appears at a relatively high temperature or at an enhanced reducing atmosphere. This reducing atmosphere probably resulted from the reducing product of the in situ PAM in the gel-like precursor during the thermal decomposition reaction.

The effect of sintering time on the amount of Fe_2P in Fe_2P–$LiFePO_4$ composites was investigated. Fe_2P–$LiFePO_4$ composites were synthesized at 750 °C for different lengths of time (6, 12, 16, 20, and 24 h) with the same in situ PAM precursor. Figure 2b shows the XRD pattern of the in situ PAM samples and the conventional PAM sample. All the in situ PAM samples are well-ordered olivine $LiFePO_4$ with a minor phase of Fe_2P. It is clear that an olivine structure was maintained upon increasing the sintering time from 6 to 24 h. Although no obvious changes in the intensity of the diffraction peak were observed for $LiFePO_4$ phase, the intensity of the Fe_2P phase (40°, 44°, and 47°) initially increased with sintering time in the range from 6 to 20 h and decreased afterward. The highest amount of Fe_2P was found at 20 h. This semi-quantitative analysis of Fe_2P was performed by the direct comparison method for the integrated intensity of reflection of $LiFePO_4$ and Fe_2P. For comparison, the conventional PAM sample was sintered at 750 °C for 20 h. However, the Fe_2P phase was not observed around $2\theta = 40°$. In addition, some other impurity (around 33° and 35°) appeared, which was probably Fe_2O_3. This indicated that simply incorporated commercial PAM could not provide sufficient reducing atmosphere during the heat-treatment process, therefore resulting in impurity contamination.

The FE-SEM images of the pure co-precipitation and in situ PAM precursor are compared in Fig. 3. It can be seen that the pure co-precipitation (Fig. 3a) was composed of nanometer-sized particles (≤100 nm) with irregular shape. After the PAM gelation reaction, the powder morphology (Fig. 3b) was different than the previous one. The in situ PAM precursor became finer, and the particles

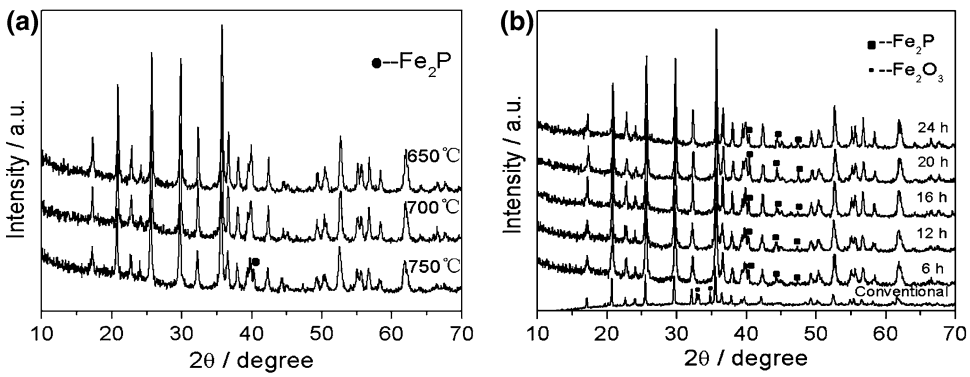

Fig. 2 XRD pattern of **a** $LiFePO_4$ prepared at various temperatures for 12 h and **b** conventional $LiFePO_4$ and Fe_2P–$LiFePO_4$ composites prepared at 750 °C for different lengths of time

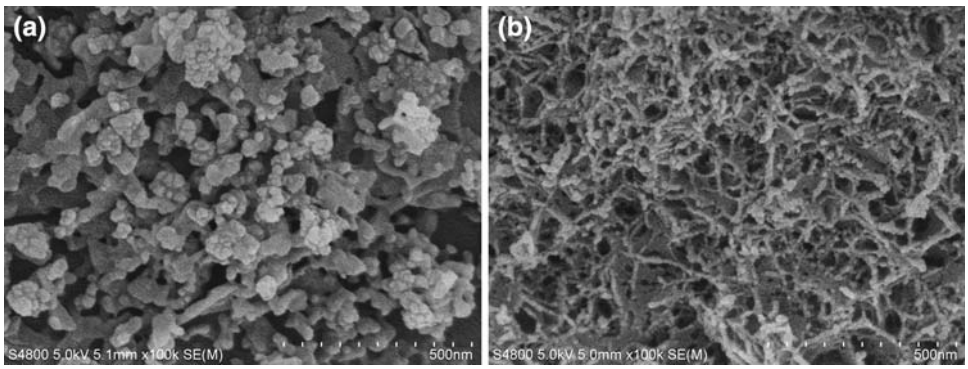

Fig. 3 FE-SEM images of **a** the pure co-precipitation and **b** the in situ PAM precursor

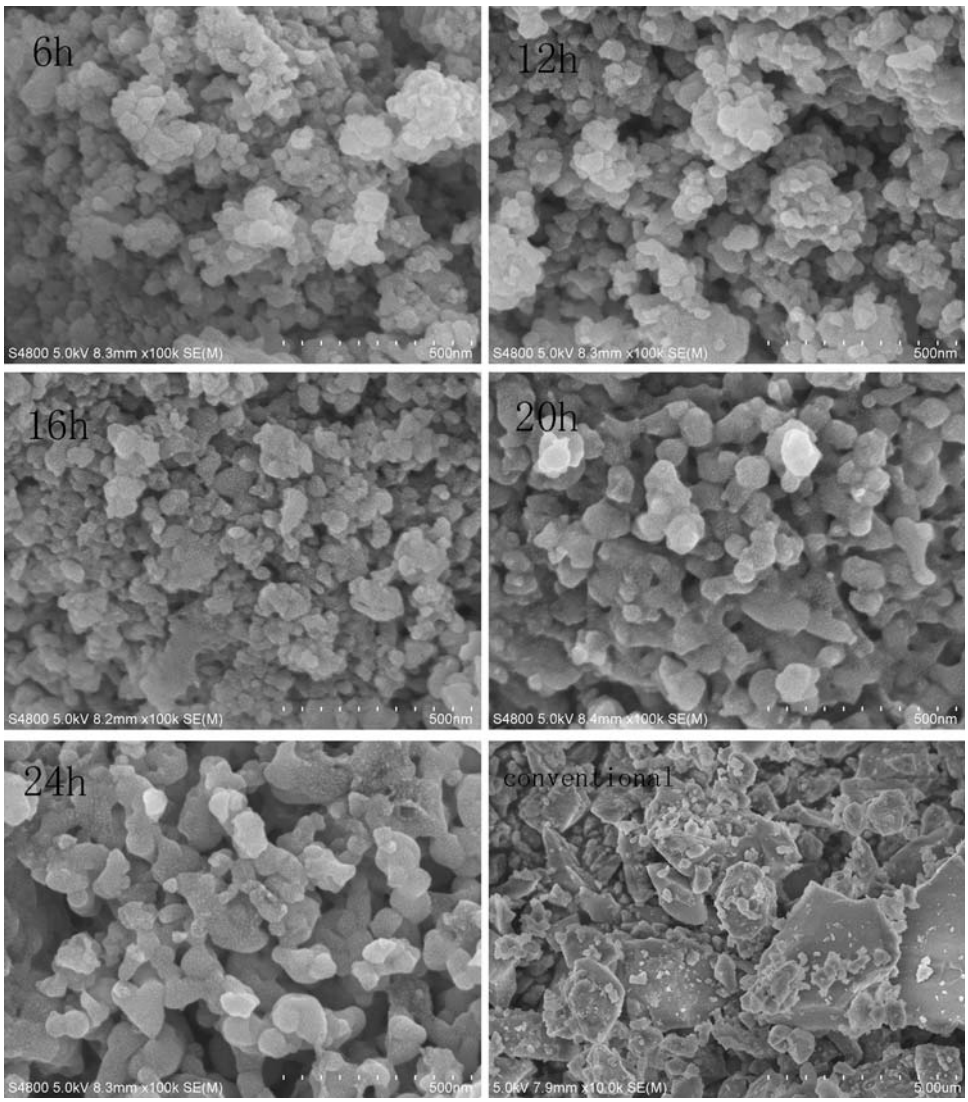

Fig. 4 FE-SEM images of conventional $LiFePO_4$ and Fe_2P–$LiFePO_4$ composites prepared at 750 °C for different lengths of time

seemed to be connected with the PAM network, which may be related to the formation of a homogeneous gel resulting from the PAM gelation reaction.

The FE-SEM images of the Fe_2P–$LiFePO_4$ composites sintering for different lengths of time were used to evaluate the effect of different heat-treatment time on the morphological change in the material. Figure 4 shows that the surface morphologies of the conventional PAM sample and Fe_2P–$LiFePO_4$ composites sintered at 750 °C with various heat-treatment time. All the Fe_2P–$LiFePO_4$ composites were composed of comparatively fine particles, and the homogeneous network shape of the precursor vanished

in the samples because the phenomenon of agglomeration became more obvious at a sintering temperature of 750 °C. The images of the three samples sintered for 6, 12, and 16 h are similar, and the particle size ranged from 50 to 120 nm. With the increasing sintering time, the particle size gradually increased. As the sintering time increased to 20 and 24 h, a moderate increase in particle size and inhomogeneous morphology was observed. The powder became more coarsened for the sample sintered for 24 h. The particle size ranged from 100 to 300 nm. As is known, the main problems of $LiFePO_4$ are low electronic conductivity and slow lithium ion diffusion. The small $LiFePO_4$ particle character ensures a large surface area for the reaction phase and reduces the diffusion length of the lithium ion, resulting in fast reaction and diffusion kinetics. On the base of the above analysis of the results, the suitable sintering time for sintering Fe_2P–$LiFePO_4$ composites should be within 20 h, and the average particle size of the 20 h sample is around 120 nm. As for the conventional PAM sample, the particle size was considerably large, with a size range of 0.5–3 μm, which indicated that the conventional PAM could not suppress the grain growth during the sintering process. In contrast, the in situ PAM not only provided the reducing atmosphere to form Fe_2P but also helped to prohibit grain growth and agglomeration of nanoparticles.

3.2 Electrochemical properties

The samples with different grain sizes and amounts of Fe_2P show different electrochemical performance. The specific capacity of the conventional PAM sample and in situ PAM samples was determined by the discharge test at 0.2 C in the voltage range of 2.5–4.2 V. As illustrated in Fig. 5, voltage plateaus of the samples were observed at around 3.4 V in the curves, indicating that the charge and discharge reactions were two phase reactions between $FePO_4$ and $LiFePO_4$. The discharge capacity increased with increasing sintering time in the time range of 6–20 h. In the process of synthesizing the Fe_2P–$LiFePO_4$ composite, the presence of a reducing agent was beneficial to the formation of Fe_2P phase. This is favorable for the formation of the reducing atmosphere with prolonging the sintering time due to the gradual decomposition of the PAM gel-like precursor. The discharge capacities of the 6, 12, and 16 samples were 95, 110, and 114 mAh g^{-1}, respectively. The 20 h sample had an initial discharge capacity of 131 mAh g^{-1}, which was due to the increased amount of Fe_2P. Fe_2P can give rise to the enhanced electronic conductivity in Fe_2P–$LiFePO_4$ composites. When the sintering time was greater than 20 h (e.g., 24 h), the reducing agent might not have been sufficient to produce Fe_2P phase any longer; therefore, the amount of Fe_2P in the 24 h sample decreased relatively. Furthermore, the particle size became larger, which, in turn, decreased the discharge capacity. As for the conventional PAM sample, the specific discharge capacity was 76 mAh g^{-1}, which was inferior to the in situ PAM sample probably due to the absence of conductive phase Fe_2P and the contamination of Fe_2O_3 impurity. In addition, the particle size of the conventional PAM sample was very large, which caused serious transport problems and hence resulted in the lower discharge capacity.

Figure 6 shows the cycling performance of all the Fe_2P–$LiFePO_4$ composites and the conventional PAM sample at 0.2 C. The sample sintered for 20 h had the largest discharge capacity and a more stable cycle life compared to the other samples. The initial discharge capacity was 131 mAh g^{-1}, and 130 mAh g^{-1} was still maintained after 30 cycles, which indicated the excellent capacity retention. In contrast, the other samples sintered for 6, 12, and 16 h had lower discharge capacities of no more than 120 mAh g^{-1}, but they also showed a good cycling performance. This demonstrated that good electrochemical performance depended on the amount of Fe_2P to a certain extent, which

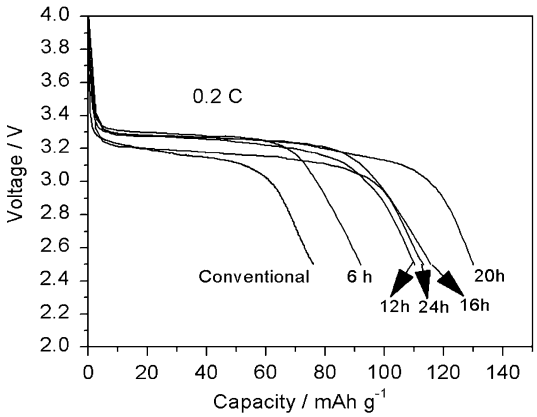

Fig. 5 The discharge curve of conventional $LiFePO_4$ and Fe_2P–$LiFePO_4$ composites prepared at 750 °C for different lengths of time

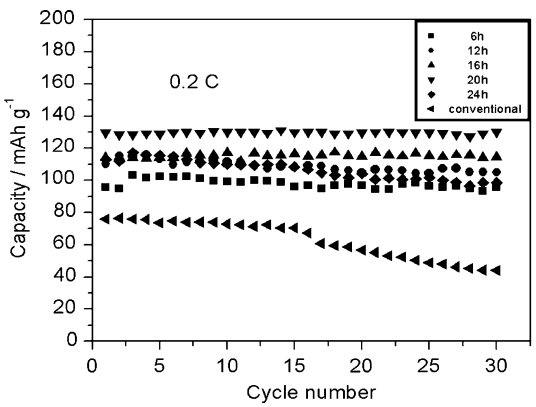

Fig. 6 Cycle performance of conventional $LiFePO_4$ and Fe_2P–$LiFePO_4$ composites prepared at 750 °C for different lengths of time

was illustrated in Fig. 2b. As for the 24 h sample, it had a slightly diminished capacity retention, which could be ascribed to the larger particle size. This result is consistent with the study of Yamada et al. [13], who reported that undesirable particle growth resulted in low utilization of the theoretical capacity at room temperature. In the case of the conventional PAM sample, it showed an initial capacity of 76 mAh g^{-1}, which was reduced to 44 mAh g^{-1} after 30 charge/discharge cycling tests. Such capacity fading of the conventional PAM sample could be attributed to the slow diffusion of Li-ions in the $LiFePO_4$ and the absence of conductive phase Fe_2P. This indicated the advantage of the Fe_2P–$LiFePO_4$ composite formed from the in situ PAM formation method.

The Fe_2P–$LiFePO_4$ composite sintered at 750 °C for 20 h not only had a good rate capability but also maintained excellent cycling stability. As shown in Fig. 7, at a C rate of 0.2 C, the electrochemical capacity was 131 mAh g^{-1}. When the C rate was increased to 0.5 C, the capacity decreased to about 120 mAh g^{-1}, and the value was about 110 mAh g^{-1} at 1 C. The capacity of the sample decreased almost linearly with increasing discharge rate. The relatively good rate performance and excellent cycle performance should be attributed to its high electronic conductivity of the Fe_2P–$LiFePO_4$ composite resulting from the Fe_2P phase and the novel synthesis process.

As for our best sample (131 mAh g^{-1} at 0.2 C, 110 mAh g^{-1} at 1 C), the carbon content of Fe_2P–$LiFePO_4$ composites were also analyzed by elemental analysis, and the amount of residual carbon in the 20 h sample was 4.48%. Taking it into account, the accurate specific capacity was 137 mAh g^{-1} at 0.2 C, which is a relatively good electrochemical performance. It still needs to be improved. Although the incorporation of the conductive phase of Fe_2P into $LiFePO_4$ is a good way to improve the electrochemical properties, in order to approach the theoretical specific capacity (170 mAh g^{-1}), the amount of Fe_2P in Fe_2P–$LiFePO_4$ composite should be optimized. Recognizing this, the amount of the Fe_2P in the best sample was probably not the optimal one. In addition, the homogeneous Fe_2P coating on the surface of the $LiFePO_4$ particles is associated with good rate capability. In our sample, Fe_2P phase was probably randomly dispersed around the $LiFePO_4$ phase rather than homogeneously coated on the surface of the $LiFePO_4$ phase; therefore, it reduced the discharge capacity. We expect that the results will be encouraging if the two weak points mentioned above can be overcome. This work is underway in our lab.

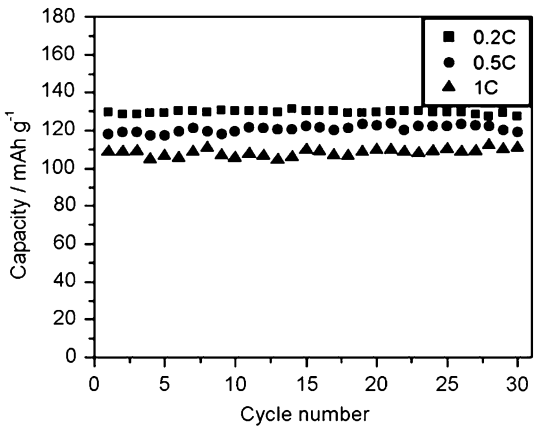

Fig. 7 Cycle performance of Fe_2P–$LiFePO_4$ composite prepared at 750 °C for 20 h at different C rates

4 Conclusions

Fe_2P–$LiFePO_4$ composites were successfully prepared by a method consisting of co-precipitation modified with in situ PAM formation. Through the in situ PAM gelation reaction, the as-prepared precursor became finer and more uniform. The pyrolysis of the in situ PAM precursor produced a strongly reductive atmosphere to ensure the synthesis of Fe_2P–$LiFePO_4$ composite. The amount of Fe_2P phase increased with increasing sintering time and reached its peak at 20 h. The Fe_2P–$LiFePO_4$ composite sintered at 750 °C for 20 h had the largest initial capacity of 131 mAh g^{-1} at 0.2 C and showed excellent cycling performance. It exhibited improved electrochemical performance compared to the sample prepared by the conventional PAM method. It also displayed comparatively good rate performance of 110 mAh g^{-1} at 1 C, which should be due to the enhanced electronic conductivity of the materials resulting from the in situ generated Fe_2P in $LiFePO_4$ and the novel synthesis process. From this point of view, it can be anticipated that the same process should be readily extendable to other olivines, such as $LiMnPO_4$ and $LiCoPO_4$, and also to other phosphates.

References

1. Schalkwijk WA, Scrosati B (2002) Advances in Lithium-ion batteries. Kluwer, New York
2. Xie HM, Wang RS, Ying JR, Zhang LY, Jalbout AF, Yu HY, Yang GL, Pan XM, Su ZM (2006) Adv Mater 18:2609
3. Padhi AK, Nanjundaswamy KS, Goodenough JB (1997) J Electrochem Soc 144:1188
4. Huang H, Yin SC, Nazar LF (2001) Electrochem Solid State Lett 4:A170
5. Barker J, Saidi MY, Swoyer JL (2003) Electrochem Solid State Lett 6:A53
6. Croce F, Epifanio AD, Hassoun J, Deptula A, Olczac T, Scrosati B (2002) Electrochem Solid State Lett 5:A47
7. Park KS, Son JT, Chung HT, Kim SJ, Lee CH, Kang KT, Kim HG (2004) Solid State Commun 129:311

8. Chung SY, Bloking JT, Chiang YM (2002) Nat Mater 1:123
9. Herle PS, Ellis B, Coombs N, Nazar LF (2004) Nat Mater 3:147
10. Doeff MM, Hu YQ, McLarnon F, Kostecki R (2003) Electrochem Solid State Lett 6:A207
11. Kim CW, Park JS, Lee KS (2006) J Power Sources 163:144
12. Kang HC, Jun DK, Jin B, Jin EM, Park KH, Gu HB, Kim KW (2008) J Power Sources 179:340
13. Yamada A, Chung SC, Hinokuma K (2001) J Electrochem Soc 148:A224
14. Hu YQ, Doeff MM, Kostecki R, Finones R (2004) J Electrochem Soc 151:A1279
15. Yang SF, Zavalij PY, Whittingham MS (2001) Electrochem Commun 3:505
16. Myung ST, Komaba S, Hirosaki N, Yashiro H, Kumagai N (2004) Electrochim Acta 49:4213
17. Arnold G, Garche J, Hemmer R, Strobele S, Vogler C, Wohlfahrt-Mehrens A (2003) J Power Sources 119:247
18. Mohan YM, Premkumar T, Lee K, Geckeler KE (2006) Macromol Rapid Commun 27:1346
19. Wang C, Flynn NT, Langer R (2004) Adv Mater 16:1074
20. Lu Y, Spyra P, Mei Y, Ballauff M, Pich A (2007) Macromol Chem Phys 208:254
21. Yang ST, Zhao NH, Dong HY, Yang JX, Hue HY (2005) Electrochim Acta 51:166
22. Ong CW, Lin YK, Chen JS (2007) J Electrochem Soc 154:A527